International Journal of Fracture **104:** 89–103, 2000.

A method for dynamic fracture toughness determination using short beams

G. WEISBROD and D. RITTEL*
Faculty of Mechanical Engineering, Technion, Haifa 32000, Israel
**author for correspondence (e-mail: merittel@tx.technion.ac.il)*

Received 18 November 1999; accepted in revised form 7 January 2000

Abstract. This paper deals with dynamic fracture toughness testing of *small* beam specimens. The need for testing such specimens is often dictated by the characteristic dimensions of the end product. We present a new methodology which combines experimentally determined loads and fracture time, together with a numerical model of the specimen. Calculations are kept to a minimum by virtue of the linearity of the problem. The evolution of the stress intensity factor (SIF) is obtained by convolving the applied load with the calculated specimen response to unit impulse force. The fracture toughness is defined as the value of the SIF at fracture time. The numerical model is first tested by comparing numerical and analytical solutions (Kishimoto et al., 1990) of the impact loaded beam. One point impact experiments were carried out on of commercial tungsten base heavy alloy specimens. The robustness of the method is demonstrated by comparing directly *measured* stress intensity factors with the results of the hybrid experimental-numerical *calculation*. The method is simple to implement, computationally inexpensive, and allows testing of large sample sizes, without restriction on the specimen geometry and type of loading.

Key words: Dynamic fracture, short beam, one point impact, tungsten base heavy alloy.

1. Introduction

By contrast with static fracture toughness (K_{Ic}) determination, the methodology for dynamic fracture toughness (K_{Id}) characterization is not yet standardized, and appropriate approaches must be devised. First, the accurate determination of the dynamic stress intensity factor(s) must take into account inertial effects (Kalthoff et al., 1977; Freund, 1990). Various methods are employed, ranging from direct crack-tip observations (e.g., Beinert and Kalthoff, 1981; Mason et al., 1990) to hybrid experimental-numerical methods (Kobayashi, 1987; Bui et al., 1992). One very important issue is the assessment of the onset of crack propagation (fracture time), which determines the fracture toughness of the material. Fracture detection relies on various methods, e.g. crack-tip monitoring using high speed photography, single wire fracture gages (Rittel et al., 1992), strain gages, and/or computer assisted fracture detection (Maigre and Rittel, 1996).

One additional problem, which is seldom mentioned in the literature is that of *specimen size limitations.* Such limitations arise from manufacturing considerations, when the emphasis is put on testing specimens extracted from the final product rather than companion specimens. In this context, the 'simplest' specimen which can be tested is the cracked beam (Bonenberger et al., 1993; Rokach, 1994). Kishimoto et al. (1990) provided an analytical evaluation of the dynamic stress intensity factor, with the restriction that the beam be dimensioned such as to

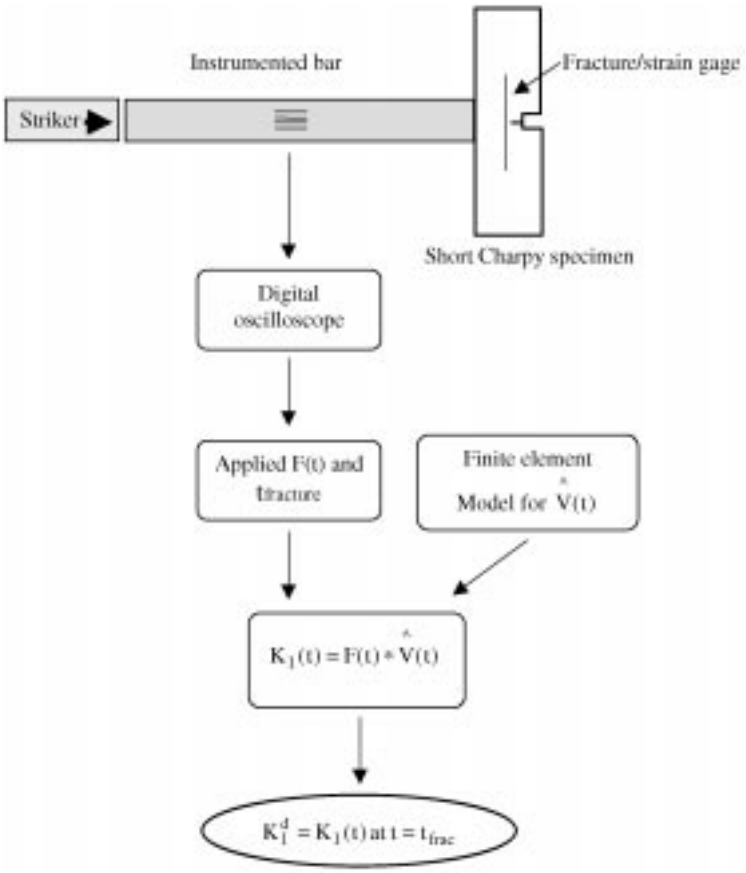

Figure 1. Schematic representation of the methodology for fracture toughness determination of short cracked beams. The fracture time and applied load are determined from the experiment. The unit impulse response of the system is calculated separately using a finite element model. The evolution of the stress intensity factor, until fracture, is determined by a convolution product between the input force and the calculated response to unit impulse.

obey Euler–Bernouilli assumptions. Such beams have been successfully tested in one point impact experiments by Kalthoff et al. (1983) and by Giovanola (1986).

In this paper, we present our approach to the dynamic fracture testing of *short beams* which cannot be considered as Euler-Bernouilli beams. The method relies on a hybrid experimental-numerical analysis of the short beam. The paper is organized as follows: first, the experimental and the numerical aspects of the approach are presented. The following section presents numerical results, including a comparison with Kishimoto's et al. (1990) results. Next, experimental and numerical results are presented and compared to validate the proposed methodology. The approach is discussed in the next section, followed by concluding remarks.

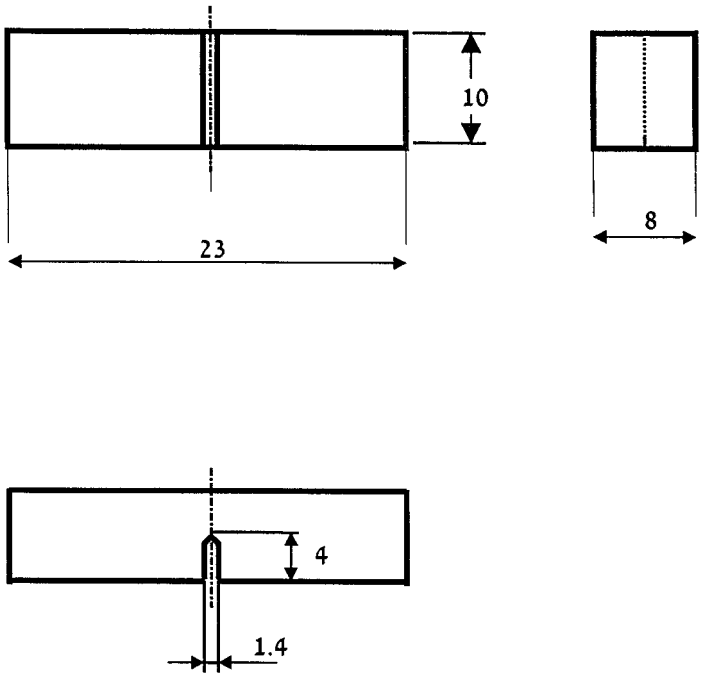

Figure 2. The short Charpy specimen (all dimensions in mm).

2. The experimental setup

2.1. Overview

An overview of the method, including the experimental setup, are shown in Fig. 1.The unsupported cracked beam specimen is loaded by stress waves. The experimental parameters are the *loads* applied to the specimen and the *fracture time* (onset of crack propagation). These parameters are subsequently used in the numerical model to determine the fracture toughness, i.e. the value of the stress intensity factor at fracture time. The various components of the experimental setup are detailed next.

2.2. Dynamic loading apparatus

Dynamic loads are applied and measured using a single instrumented bar (Kolsky, 1963), to perform one point impact experiments (Kalthoff et al., 1983; Giovanola, 1986; Rittel, 1998).The apparatus consists of a cylindrical incident bar (750 mm long, 10 mm diameter), instrumented at its mid-length with a pair of diametrically cemented strain gages. Stress wave loading is applied by means of an air propelled cylindrical striker. The length of the striker and its velocity at impact set the duration and amplitude of the stress wave which loads the fracture specimen. Both the incident bar and the striker are made of a commercial tungsten base heavy alloy (w/o-90W-7Ni-3Fe). The specimen lays unsupported, and is in contact with the bar. Consequently, fracture results from inertia only, as typical of one point bend (1PB) impact fracture (Giovanola, 1986).

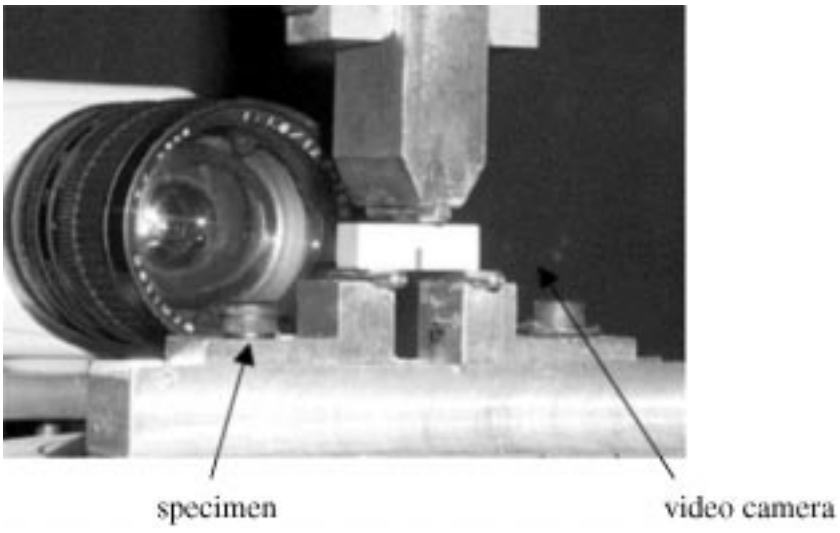

Figure 3. The three point bending setup for fatigue precracking.

Table 1. Measured mechanical properties of the heavy alloys base tungsten

	Young's modulus (GPa)	Poisson's ratio
Dynamic	338	0.3

2.3. SPECIMEN AND MATERIAL

The experimental specimens are of the *short* Charpy type, whose geometry and dimensions shown in Fig. 2. All the specimens were fatigue precracked on a servo-hydraulic machine (MTS-810), according to ASTM standard recommendations (ASTM-E399, 1993). Crack growth monitoring was carried out by means of two video cameras (Fig. 3).

The experimental material was a commercial tungsten base heavy alloy (w/o-90W-7Ni-3Fe), whose properties (as measured in our laboratory) are listed in Table 1. The density was found to be $\rho = 17100$ kg/m^3. Poisson's ratio was determined for two orthogonal specimen orientations with respect to the applied load. These measurements showed very little difference between the two directions so that the material can reasonably be considered as isotropic for computational purposes. Young's modulus was determined from the measured longitudinal wave velocity in the incident bar. This value represents the dynamic Young's modulus which is used in numerical calculations to accurately reproduce wave propagation in the specimen (Wada, 1992; Rittel and Maigre, 1996).

2.4. IMPACT LOAD DETERMINATION

When the striker hits the incident bar, a strain pulse (ε_{in}) propagates down the bar. Part of this pulse is reflected (ε_{ref}) at the specimen-bar interface, and part of it is transmitted to the specimen. The incident and reflected pulses were corrected for geometrical dispersion and attenuation using standard data reduction techniques (Lifhitz and Leber, 1994).

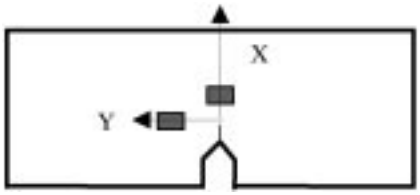

Figure 4. Schematic representation of the short beam with two strain gages at $\theta = 0$ and $\theta = \pi/2$.

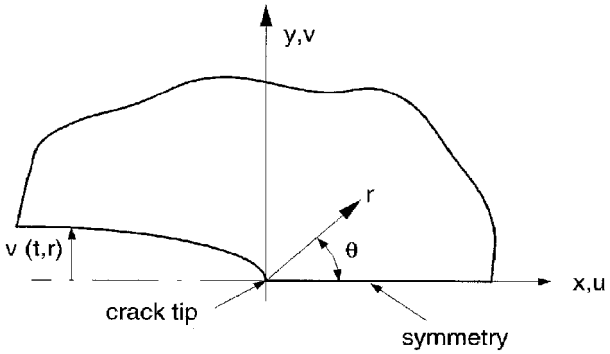

Figure 5. The crack-tip, coordinate system. The displacement $V(t)$ is calculated at a distance r and $\theta = \pi$.

The incident load $F(t)$ was determined from these two pulses, using the one-dimensional theory of elastic wave propagation as:

$$F(t) = AE\left[\varepsilon_{\text{in}}(t) + \varepsilon_{\text{ref}}(t)\right], \tag{1}$$

where E is Young's modulus and A is the cross-sectional area of the incident bar.

2.5. Determination of fracture time t_f

The onset of crack propagation was detected, in most experiments, by means of single wire fracture gages (MM CD-02-10A) cemented on each side of the specimen, under the optical microscope. The distance between the crack-tip and the fracture gage was kept to a minimum ($d \approx 0.1$ mm).

Since accurate fracture time determination is essential, several experiments were carried out with one fracture gage cemented on one side and a 0.2 mm strain gage (KYOWA KFG-02-120) on the other side. The strain gage was located at a distance which varied from 0.5mm to about 1mm from the crack-tip, and angles of $\theta = 0$ or $\theta = \pi/2$, as shown in Fig. 4. This distance was selected, both for the strain gage to be located outside the presumed plastic zone, and also to minimize the experimental error associated with strain gradients in the singular zone (Dally and Riley, 1991). When strain gages cemented at $\theta = \pi/2$ are used, crack extension manifests itself either by a noticeable drop in the measured strain or by a gradual deviation from linearity, according to Giovanola (1986).

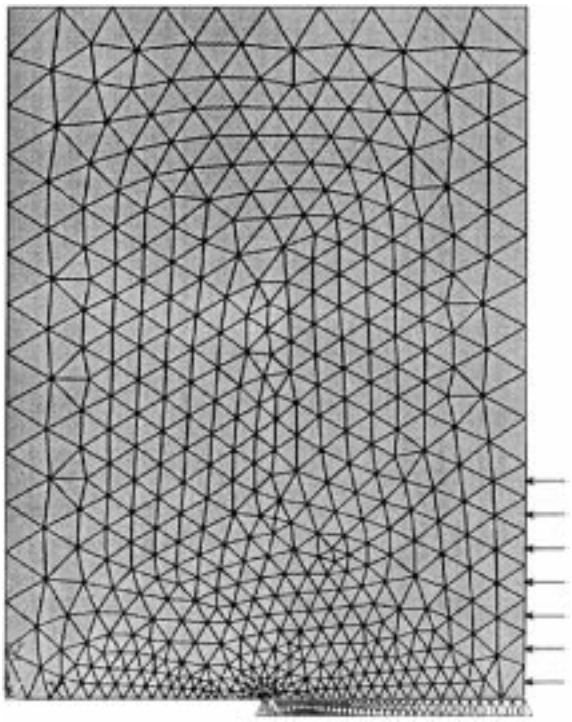

Figure 6. The meshed half-specimen for finite element analysis. The load is applied as a pressure along the specimen-bar interface. The specimen is unconstrained.

3. Determination of dynamic fracture toughness $K\,I\,d$

3.1. Finite element model

The dynamic fracture toughness KId is defined as the value of the mode I stress intensity factor (SIF) at the fracture time. The SIF was calculated from Irwin's (1957) formula which relates the crack opening displacement (COD) to the SIF. The expression for plane strain is:

$$\mathrm{COD}(t)_{(r,\theta=\pi)} = K_I(t)\frac{8(1-\nu^2)}{E}\sqrt{\frac{r}{2\pi}}. \tag{2}$$

Defining $V(t) = \mathrm{COD}(t)/2$, the symmetry of the problem yields (Fig. 5):

$$K_I(t) = \frac{V(t)E}{4(1-\nu^2)}\sqrt{\frac{2\pi}{r}}, \tag{3}$$

where $V(t)$ is the displacement of a selected point located at a distance r and $\theta = \pi$ from the crack tip. V(t) was determined by solving the equation of motion of the dynamically loaded *free* specimen, with a *stationary* crack:

$$[M]\{\ddot{V}\} + [K]\{V\} = F(t), \tag{4}$$

where $[K]$ and $[M]$ are the assembled stiffness and mass matrices, respectively, and $F(t)$ is the external force vector. Equation (4) was solved using Newmark time integration method (Bathe, 1982) using the commercial finite element code, ANSYS (ANSYS, 1994). The time increment

was set to 0.5 μs. Due to symmetry considerations, a two dimensional representation of half the specimen was adopted. Plane strain conditions were assumed, and the material was modeled as linear-elastic. The load was applied to the unconstrained specimen as a pressure along the contact (specimen-bar interface) line, to simulate actual experimental conditions. It was also modeled as a point force to replicate the analytical case of the point loaded beam, as discussed in the sequel. The crack-tip singularity was enforced by quarter point six-nodes trianglular isoparametric element (Barsoum,1978).The discretized specimen (684 elements and 2113 nodes) is shown in Fig. 6. Finer mesh sizes were tested in order to examine the effect of mesh size. It was observed that finer meshes did not yield significantly different results.

3.2. Determination of the SIF by convolution integral

The dynamic SIF can be computed for any applied load by a finite element simulation of the experiment. However, this is time consuming, and thus not quite appropriate for large scale laboratory testing. Fortunately, the linearity of the problem can be advantageously used by writing:

$$V(t) = F(t) * \hat{V}(t), \tag{5}$$

where $F(t)$ is the experimentally determined force, and $\hat{V}(t)$ is the numerically determined response (COD) of the specimen to a unit impulse (point or pressure) load. The sign $*$ indicates a time convolution product.

The first advantage of this procedure is that, for a given crack length, $\hat{V}(t)$, is only calculated once, while Equation (5) is used as many times as necessary. It must also be emphasized that this method is not restricted to a given specimen (beam) geometry or load distribution.

4. Results

To validate the approach proposed here, we present three kinds of results. The first is purely numerical and it pertains to the accuracy of the numerical model. The second is a comparison of numerical and analytical results for a dynamically loaded cracked beam. Finally, we present and compare experimental results and numerical simulations.

4.1. Numerical results: convolution vs. full calculation

Fig. 7 shows the unit impulse response, $\hat{V}(t)$, calculated for a crack length of 5 mm, at $r = 0.5$ mm and $\theta = \pi$. A semi-sinusoidal force, $F(t)$ (40 μs duration, 15 KN max.), was selected to simulate a transient load applied to the structure. The resulting COD was calculated using both the full FE calculation and the convolution product (Equation (5)). As shown in Fig. 8, both methods show an excellent agreement, a result which is expectable in a sense.

4.2. Comparison with analytical solution

Kishimoto et al. (1990) derived an analytical solution for the evolution of the stress intensity factor of a dynamically loaded beam. This solution is limited to concentrated load applied to an Euler-Bernouilli beam. Our short beam specimens do not obey this last assumption. However, as suggested by these authors, the analytical solution can still be used, provided the correct natural frequencies of the specimen are calculated. The latter were thus calculated for

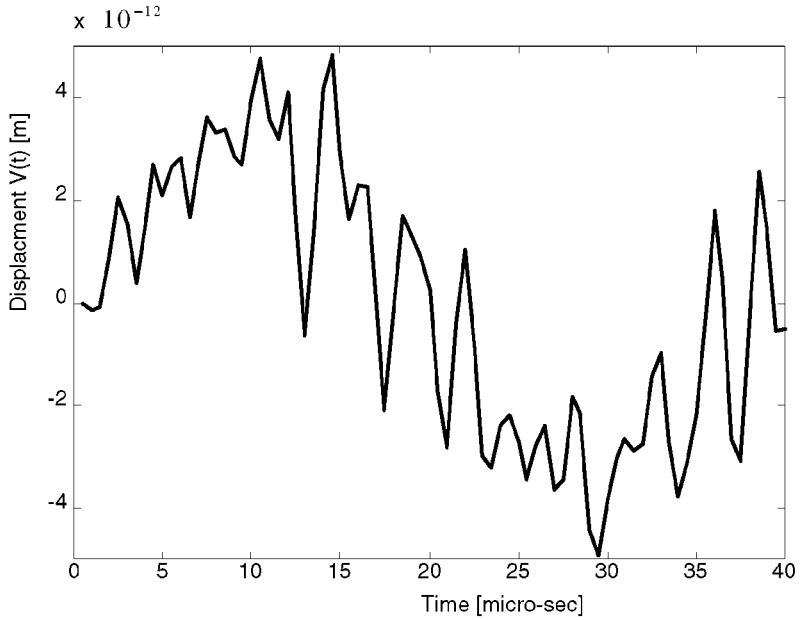

Figure 7. The response $\hat{V}(t)$ to unit impulse point force.

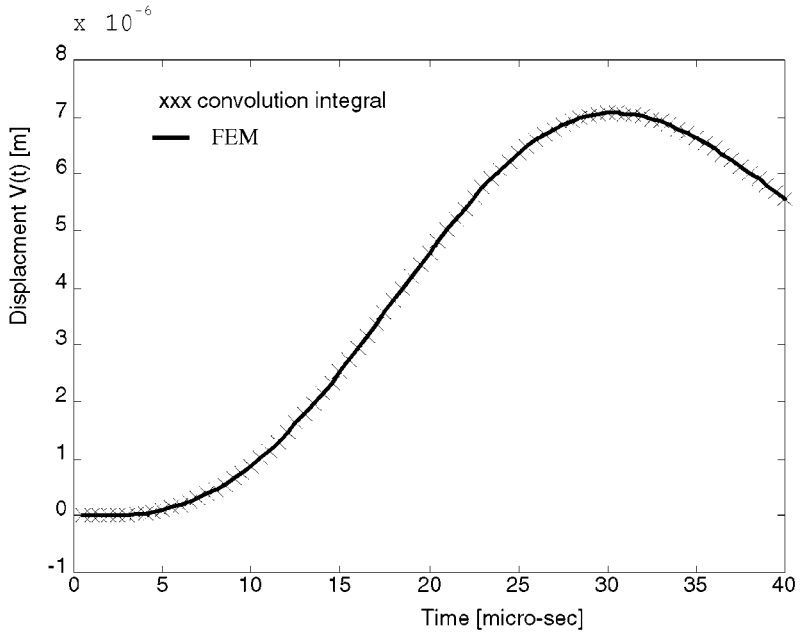

Figure 8. Evolution of the displacement $V(t)$, as a result of a half-sine transient load. $V(t)$ is calculated, once through a full finite element solution, and once through the convolution integral (Equation (5)). The two calculations yield identical results.

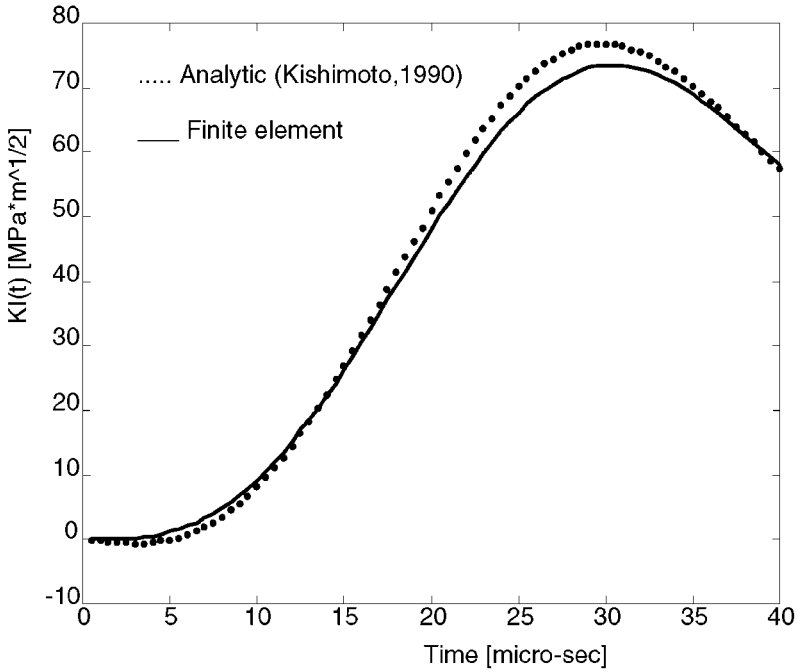

Figure 9. Numerical results. Calculated evolutions of the stress intensity factor, using once a full finite element calculation, and once Kishimoto's et al. (1990) analytical solution with the correct calculated angular frequencies of the short beam.

the numerical model. A comparison between the full finite element solution and Kishimoto's et al. (1990) solution, including the correct angular natural frequencies, is shown in Fig. 9. A very good agreement between the analytical and numerical results can be observed. The minute difference between the curves stems from the fact that the discretized model is more rigid than the continuous beam on the one hand, and that Euler-Bernouilli assumptions still apply to the analytical solution on the other hand.

4.3. Comparison with experimental results

Experiments were carried out with a characteristic crack to ligament length ratio of $a/w = 0.5$. Typical raw experimental signals are shown in Fig. 10. This includes the incident (ε_{in}) and reflected (ε_{ref}) pulses, and the fracture and strain gage signals as well. In this specific experiment, the strain gage was positioned at $r = 1$ mm and $\theta = 0$. All the signals are synchronized. The incident pulse starts at $t = 71$ μs and the reflected at $t = 239$ μs. Consequently, the specimen is loaded by the stress wave at $t = 155$ μs. The strain and fracture gage signals are shown in Fig. 11. This figure shows that fracture is detected at $t = 21$ μs after the specimen was impinged upon by the stress wave. In this specific experiment, the crack arrested before reaching and destroying the strain gage. Consequently, crack propagation was assigned to occur at the time where the crack-tip strain starts to decrease. It was generally observed that the maximum difference in fracture times between the strain and the fracture gages did not exceed 3 μs.

The corresponding evolution of the applied force (Equation (1)) is shown in Fig. 12. Largely after fracture occurs, the force reaches negative values. This is unphysical and it results from the superposition of the incident and reflected pulses only (Equation (1)). Fracture

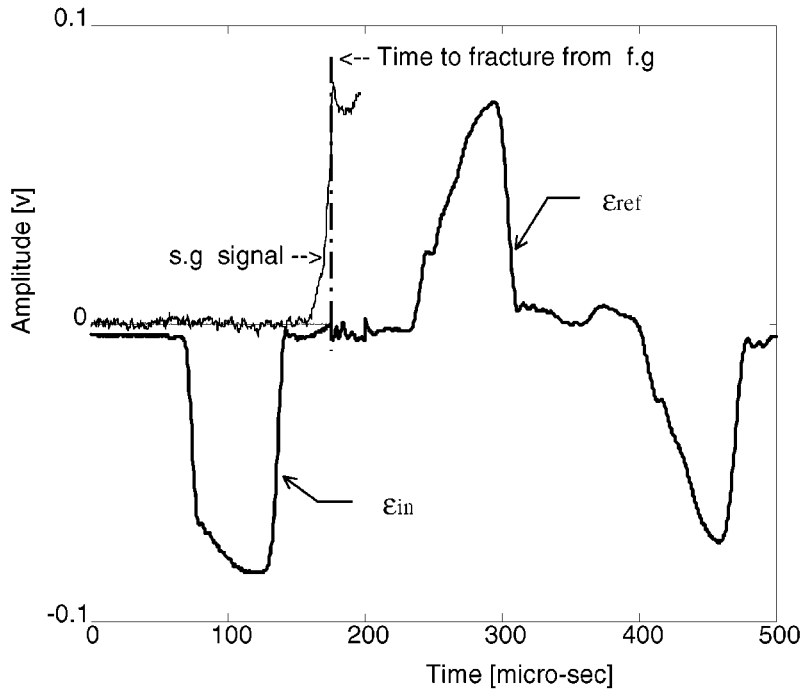

Figure 10. Characteristic raw signals obtained during a one-point impact experiment. All the signals have a common time origin but are measured at a different location. The incident and reflected signals (measured on the strain gage of the bar) are different, indicating that part of the energy has been transferred to the specimen. The single wire fracture gage indicates crack propagation (dashed line). The strain gage records the crack-tip strain from the onset of loading until, and sometimes beyond, crack propagation (depending on the angular position of the gage).

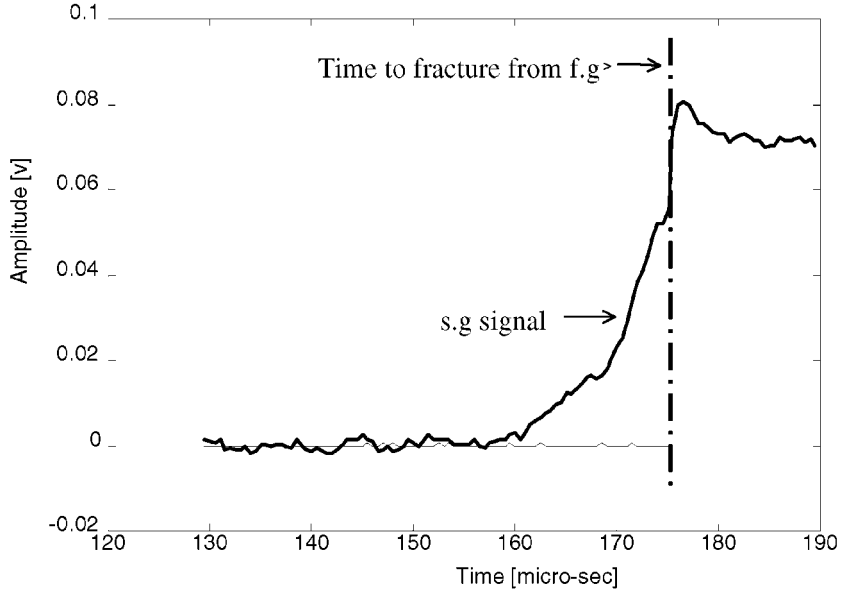

Figure 11. Magnification of the strain gage and fracture gage recording. The fracture gage delivers a step signal. Fracture is detected by the strain gage as the point at which the strain signal starts to decrease.

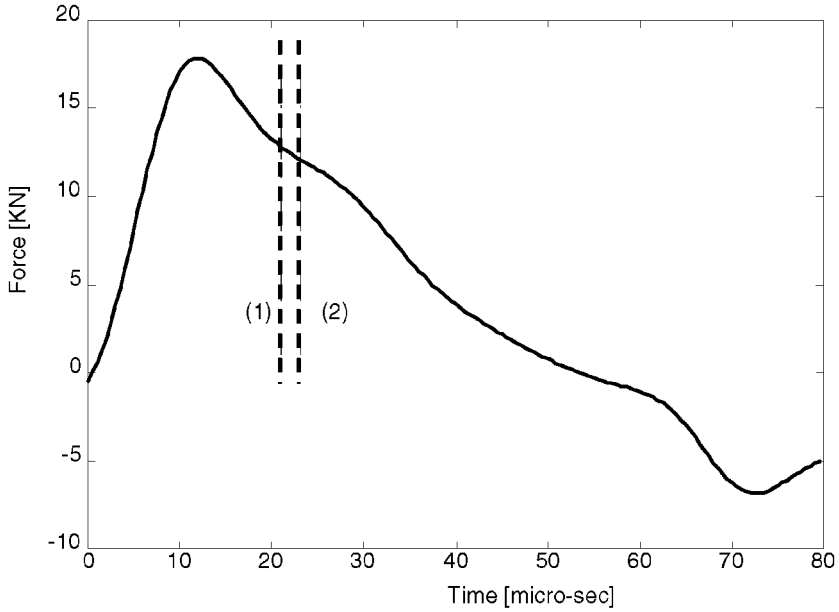

Figure 12. The applied force and the fracture times. The 1st dashed line corresponds to fracture from the fracture gage (21 μs). The 2nd dashed line indicates fracture from the strain gage (23 μs). Note that fracture occurs past the peak load.

is noted to occur beyond the peak force. This reflects the very transient nature of this kind of fracture experiment.

In Fig. 13a, we have plotted the dynamic stress intensity factor determined in two ways. The first is evaluated from the strain gage readings according to:

$$K_{I(t)} = \frac{\varepsilon_y(t) E \sqrt{2\pi r}}{\cos\frac{\theta}{2}\left[1 + \sin\frac{\theta}{2}\sin\frac{3\theta}{2} - \nu\left(1 - \sin\frac{\theta}{2}\sin\frac{3\theta}{2}\right)\right]}. \tag{6}$$

The second is calculated from the experimental force (Equation (5)). Fig. 13b shows evolutions of stress intensity factors for an additional experiment. Here the fracture gage was cemented at $r = 0.5$ mm and $\theta = \pi/2$. Fracture was detected at $t = 19.5$ μs by the fracture gage. For the strain gage reading, deviation from linearity was assessed to occur at the same time.

These figures show a high degree of similarity between the two evolutions of the stress intensity factors, until fracture. It can be noted that for an initial duration of about 7 μs, the crack is not loaded by the stress wave. Past this time, the stress intensity factor starts to increase.

This similarity validates the approach proposed here, in the sense that two different, yet complementary, procedures for the determination of the SIF corroborate mutually. In the first, the SIF is directly *measured* in the vicinity of the crack-tip. In the second, the SIF is *calculated* in a hybrid experimental-numerical procedure.

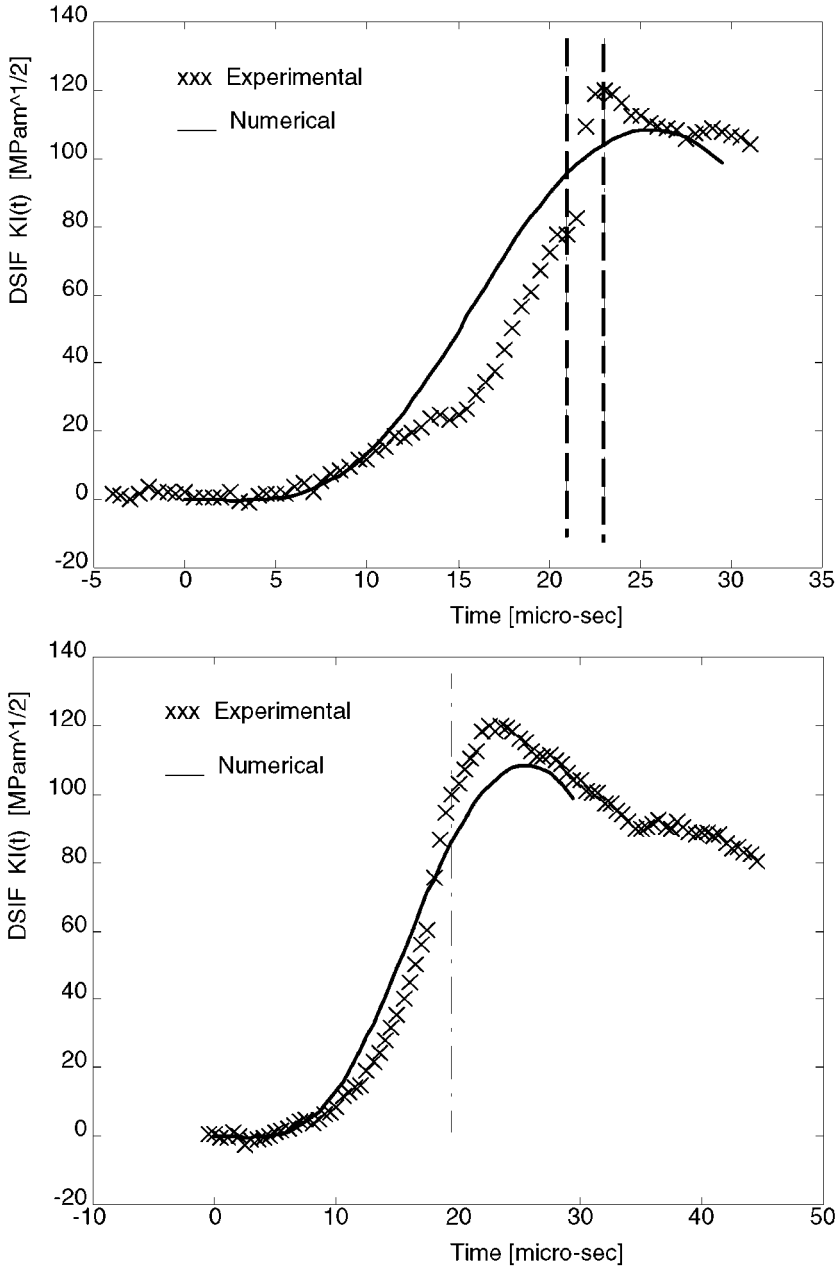

Figure 13. Calculated and measured dynamic stress intensity factors in typical experiments. Dashed lined indicate fracture time. (a) strain gage at $r = 1$ mm and $\theta = 0$. Fracture times are as indicated in Figure 12. Another experiment. Strain gage at $r = 0.5$ mm and $\theta = \pi/2$. Fracture times are similar for both indicators (19.5 μs). Note the high degree of similarity between the measured and calculated results.

5. Discussion

The method presented in this paper relies on the numerical solution of the equation of motion of the cracked specimen. The reliability of the numerical model is firstly tested by comparing its predictions with analytical. It is further established by comparing calculated and directly measured stress intensity factors. The comparison is quite satisfactory, despite the potential sources of error in each of the methods. For the direct measurement, accurate positioning of the strain gage determines the accuracy of the measurement, when errors due to strain gradient effects are minimized (Dally and Riley, 1991). For the calculation, neglecting numerical errors related to the FE model, one potential source of error lies in the determination of the input force, through the signal processing procedure. While an estimation of the relative error in each procedure is a complex task, an estimation of the error involved in the numerical determination yielded a value of 6%.

Yet, when all errors are kept to a minimum, the most important parameter is the determination of the fracture time. It has long been recognized that this is not a trivial problem, when the measurements are made on the surface of the specimen, thus excluding three-dimensional effects (Aoki and Kimura, 1993; Maigre and Rittel, 1996). In our experiments, two different indicators were used. The first, fracture gage, reacts when the crack cuts across the wire. In a sense, the fracture provides a 'go-no-go' type of indication. The second, strain gage, reacts to mechanical damage as well, but also to changes in overall compliance due to crack propagation. Here, the fracture time has to be estimated from changes in the strain signal (Giovanola, 1986), and a certain ambiguity may exist related to the interpretation of the signals. Yet, keeping in mind that the two gages are cemented, one on each side of the specimen, the measured fracture times did not differ by more than 3 μs, as observed in several different experiments. This observation shows that there is no discrepancy between the two fracture detection methods. In this case, its seems reasonable to take the earlier fracture time as the fracture time for (conservative) fracture toughness determination.

At this point, it should be emphasized that while a new methodology has been presented, the validity of a specific fracture toughness measurement can only be assessed by verifying compliance with LEFM requirements.

Finally, the method presented in this paper is easy to implement in a laboratory, and it provides accurate results with a minimum amount of numerical calculations, for a large sample size. Furthermore, it puts no restriction on the specimen geometry and size.

6. Conclusions

- We have presented a new methodology for dynamic fracture toughness testing of *small* elastic beams.
- The approach combines experimentally determined loads and fracture time together with a numerical model of the specimen.
- Calculations are kept to a minimum by virtue of the linearity of the problem. The SIF is obtained by convolving the applied load with the calculated specimen response to unit impulse force.
- The method has been firstly validated by comparing numerical and analytical results. It has been further established by comparing numerically and experimentally determined stress intensity factor evolutions.

- Fracture time detection has been assessed by fracture gage and strain gage readings. Both methods yield close values. Fracture time is taken as the minimum value of the two indications.
- The method is simple to implement, computationally inexpensive, and allows testing of large sample sizes.

Acknowledgements

Ashot-Ashkelon Industries Ltd. is acknowledged for supplying the experimental material.

References

ANSYS, User's Manual (1994). Swanson Analysis Systems Inc.

Aoki, S. and Kimura, T. (1993). 'Finite element study of the optical method of caustic for measuring impact fracture toughness'. *Journal of the Mechanics and Physics of Solids* **41** (3), 413–425.

ASTM (1993). Standard test method for plane-strain fracture toughness of metallic materials. *Annual Book of ASTM Standards*, Vol. 03.01, ASTM, Philadelphia, PA.

Bathe, K.J. (1982). *Finite Element Procedures in Engineering Analysis*, Prentice Hall Inc., Englewood Cliff, N.J.

Barsoum, R.S. (1978). 'On the use of isoparametric finite elements in linear elastic fracture mechanics'. *International Journal of Numerical Methods in Engineering* **10**, 25–37.

Beinert, J. and Kalthoff, J.F. (1981). 'Experimental determination of dynamic stress intensity factors by shadow patterns'. *Mechanics of Fracture 7* (Edited by Sih, G.C.), 281–330.

Bonenberger, R.J., Dally, J.W. and Irwin, G.R., (1993). 'Lower bound initiation toughness with a modified Charpy specimen'. *ASTM STP* **1171**, 139–157.

Bui, H.D., Maigre, H. and Rittel, D. (1992). 'A new approach to the experimental determination of the dynamic stress intensity factor'. *International Journal of Solids and Structures* **29** (23), 2881–2895.

Dally, J.W. and Riley, W.F. (1991). *Experimental Stress Analysis*, 3rd Ed., McGraw-Hill, New York.

Freund, L.B. (1990). *Dynamic Fracture Mechanics*, Cambridge University Press, Cambridge.

Giovanola, J.H. (1986). 'Investigation and application of the one-point bend impact test'. *Fracture Mechanics: Seventeenth Volume*, ASTM-STP 905 (Edited by Underwood, J.H., Chait, R. et al.), 307–328.

Irwin, G.R. (1957). 'Analysis of stresses and strains near the end of a crack traversing a plate'. *Journal of Applied Mechanics* **24** (3), 361–364.

Kalthoff, J.F., Winkler, S., Böhme, W., Shockey, D.A. (1983). Proceedings International Conference on the Dynamical Properties and Fracture Dynamics of Engineering Materials, Brno, Czechoslovakia.

Kalthoff, J.F , Winkler, S. and Beinert J. (1977). 'The influence of dynamic effects in impact testing'. *International Journal of Fracture* **13**, 528–531.

Kishimoto, K., Fujino, Y., Aoki, S. and Sakata, M. (1990) 'A simple formula for the dynamic stress intensity factor of an impacted freely supported bend specimen'. *JSME International Journal Series I*, **33** (1), 51–56.

Kobayashi, A.S. (1987). *Handbook on Experimental Mechanics*, Prentice-Hall, Inc., Englewood Cliffs NJ.

Kolsky, H. (1963). *Stress Waves in Solids*, Dover Publications Inc., New York, NY.

Lifshitz, J.M. and Leber, H. (1994). Data processing in the split Hopkinson pressure bar tests, *International Journal of Impact Engineering* **15** (6), 723–733.

Maigre, H. and Rittel D. (1996). 'Dynamic fracture detection using the force-displacement reciprocity: application to the compact compression specimen'. *International Journal of Fracture* **73** (1), 67–79.

Mason, J.J., Lambros, J. and Rosakis, A.J. (1992). 'The use of a coherent gradient sensor in dynamic mixed-mode fracture mechanics experiments'. *Journal of Mechanical Physics and Solids* **40** (3), 641–661.

Rittel, D. (1998). 'The influence of temperature on dynamic failure mode transitions'. *Mechanics of Materials* **30** (3), 217–227.

Rittel, D. and Maigre, H. (1996). 'An investigation of dynamic crack initiation in PMMA'. *Mechanics of Materials* **28**, 229–239.

Rittel, D., Maigre, H and Bui, H.D. (1992). A new method for dynamic fracture toughness testing. *Scripta Metallurgica et Materialia* **26**, 1593–1598.

Rokach, I.V. (1994). 'Comparison of simplified methods of dynamic stress intensity factor evaluation'. *Mechanika Teoretyczna I Stosowana* **1** (32), 203–212.

Wada, H. (1992). 'Determination of dynamic fracture toughness for PMMA'. *Engineering Fracture Mechanics* **41** (6), 821–831.